Anharmonic magnon excitations in noncollinear and charge-ordered $RbFe^{2+}Fe^{3+}F_6$

M. Songvilay,[1] C. Stock,[1] E. E. Rodriguez,[2] R. Lindsay,[3] M. A. Green,[3] H. C. Walker,[4] and J. A. Rodriguez-Rivera[5,6]

[1] *School of Physics and Astronomy and Centre for Science at Extreme Conditions, University of Edinburgh, Edinburgh EH9 3FD, UK*
[2] *Department of Chemistry and Biochemistry, University of Maryland, College Park, Maryland 20742, USA*
[3] *School of Physical Sciences, University of Kent, Canterbury, CT2 7NH, UK*
[4] *ISIS Neutron and Muon Source, Rutherford Appleton Laboratory, Chilton, Didcot OX11 0QX, United Kingdom*
[5] *NIST Center for Neutron Research, National Institute of Standards and Technology, 100 Bureau Drive, Gaithersburg, Maryland, 20899, USA*
[6] *Department of Materials Science, University of Maryland, College Park, Maryland 20742, USA*

(Dated: April 27, 2018)

$RbFe^{2+}Fe^{3+}F_6$ is an example of a charge ordered antiferromagnet where iron sites, with differing valences, are structurally separated into two interpenetrating sublattices. The low temperature magnetically ordered Fe^{2+} (S=2) and Fe^{3+} (S=5/2) moments form a noncollinear orthogonal structure with the Fe^{3+} site displaying a reduced static ordered moment. Neutron spectroscopy on single crystals finds two distinct spin wave branches with a dominant coupling along b-axis Fe^{3+} chain axis. High resolution spectroscopic measurements find an intense energy and momentum broadened magnetic band of scattering bracketing a momentum-energy region where two magnon processes are kinematically allowed. These anharmonic excitations are enhanced in this non collinear magnet owing to the orthogonal spin arrangement.

Quasiparticles in condensed matter are generally long-lived and non-interacting with a prototypical example being magnon excitations in ordered magnetic lattices. Classically, in the high spin limit, these excitations correspond to transverse small-angle deviations of a spin vector away from the equilibrium direction with the length of the vector remaining fixed. This distortion of the underlying magnetic lattice is harmonic and results in underdamped spin waves. However, the conditions under which these excitations breakdown has become important to understanding low energy properties in a variety of systems including superconductivity [1, 2], frustrated magnets [3–5], and also quantum liquids [6–8, 32]. We demonstrate the breakdown of this quasiparticle notion in a classical magnet with non collinear magnetic order establishing spin geometry as an ingredient establishing quasiparticle stability.

Due to enhanced phase space and also large quantum fluctuations, one-dimensional and low-spin magnets have been at the center of the search for the breakdown of conventional spin-waves into multiparticle states [9–12]. Such composite particles carry fractional quantum numbers and are observed through decay products in scattering experiments [13–16] resulting in a momentum and energy broadened continuum cross section and renormalization [17–19] of the single-magnon dispersion and intensity. In collinear square lattice antiferromagnets, spin wave theory predicts two-magnon processes, which are longitudinally polarized, and correspond to the simultaneous creation of two magnons of opposite signs, reducing the value of the ordered spin moment compared to the full value S [20]. The cross section scales as $1/S$ [17] and is inherently weak in classical high-spin magnets [21] and such processes have been generally investigated in $S = 1/2$ magnets where quantum fluctuations are large. Another means of enhancing this cross section is through a non collinear magnetic structure where longitudinal and transverse excitations are intertwined through geometry of the magnetic lattice [15, 16, 22]. In this work, we investigate such anomalous spin fluctuations in the charge ordered $RbFe^{2+}Fe^{3+}F_6$ based on an orthogonal spin geometry.

$RbFe^{2+}Fe^{3+}F_6$ crystallizes in the *Pnma* space group (Fig. 1 (a)) with the lattice parameters a =6.9663(4), b =7.4390(5) and c =10.1216(6) Å at T = 4 K. As mentioned in [23], $RbFe^{2+}Fe^{3+}F_6$ has a structure related to the α-pyrochlores $A_2B_2X_6X'$ but with a vacancy on one of the two A cations and another on the X' anion site that does not contribute to the BX_6 octahedra. Charge order in this compound originates from two different iron sites which have differing valences. The $RbFe^{2+}Fe^{3+}F_6$ structure can be described as a chain of corner-shared $Fe^{3+}F_6$ octahedra running along b and a chain of corner-shared $Fe^{2+}F_6$ octahedra running along the a-axis. The two chains are connected along the c axis to form a two dimensional network, reminiscent of a Kagome arrangement, in the (1 0 1) plane. While the $Fe^{3+}F_6$ octahedra are only slightly distorted, a substantial distortion exists on the $Fe^{2+}F_6$ octahedra likely due to the Jahn-Teller effect given the underlying orbital degeneracy for octahedrally coordinated Fe^{2+}. [24–26].

Both magnetic iron sites order antiferromagnetically below T_N=16 K with the Fe^{2+} and Fe^{3+} magnetic moments oriented 90° with respect to each other forming a noncollinear structure. As illustrated in Fig. 1 (a), the Fe^{3+} moments point along the a-axis and are coupled antiferromagnetically through nearest-neighbor interaction along the b-axis. The Fe^{2+} moments point in the orthogonal direction (b-axis) and are coupled antiferromagnetically through nearest-neighbor interac-

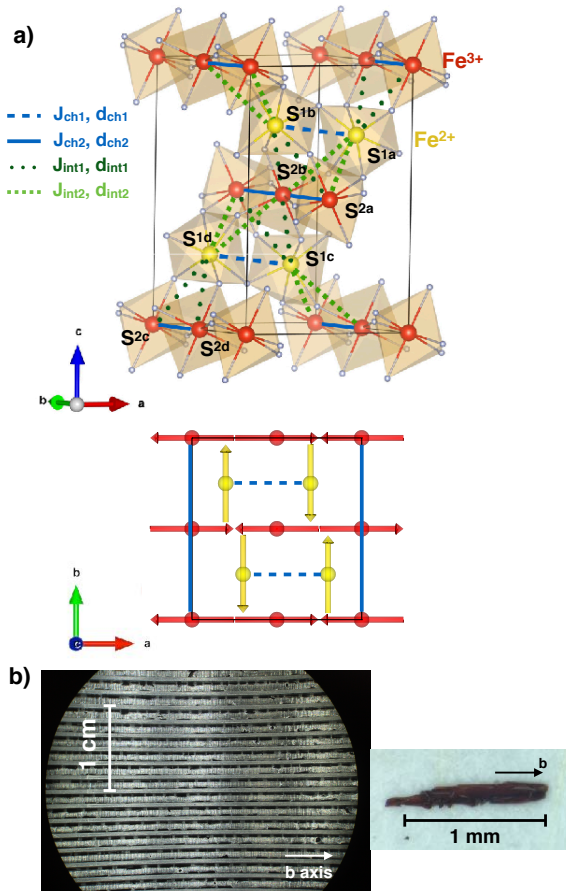

FIG. 1. (a) Crystallographic structure of $RbFe^{2+}Fe^{3+}F_6$ with the $Fe^{3+}F_6$ (red) and $Fe^{2+}F_6$ (yellow) network and view of the perpendicular arrangement of the spins in the (a, b) plane.The colored lines indicate the inequivalent nearest-neighbor exchange couplings, associated with the nearest-neighbor Fe-Fe distances. (b) Photo of the sample mounting and a single crystal of $RbFe^{2+}Fe^{3+}F_6$; the small single crystals were coaligned along the b axis.

tion along a. In the low temperature ordered state, the saturated magnetic moments measured via neutron diffraction are $m(Fe^{3+}) = 4.29(5)\mu_B$ (S = 5/2) and $m(Fe^{2+}) = 3.99(5)\mu_B$ (S = 2). Given that the expected magnetic moment is equal to gS, with g the Lande factor equal to 2, while the Fe^{2+} displays the full ordered magnetic moment the ordered magnetic moment on the Fe^{3+} is strongly reduced.

We apply neutron spectroscopic measurements to investigate the magnetic dynamics in $RbFe^{2+}Fe^{3+}F_6$. Single crystals of $RbFe^{2+}Fe^{3+}F_6$ were made using hydrothermal techniques discussed in the supplementary material. With each crystal weighing less than 1 mg, between three and five thousand were coaligned using hydrogen free Fomblin grease on a series of aluminum plates, using the long chain b-axis as a guide. The estimated total mass was between 0.3 - 0.5 g (Fig. 1 (b)). Neutron spectroscopy was performed using the MERLIN chopper spectrometer (ISIS, UK) and the MACS cold triple-axis (NIST, Gaithersburg). Further details are supplied in the supplementary information. The dynamical structure factor associated with the single magnon excitations was calculated using the SPINWAVE software [27].

We first discuss the dynamics in the low temperature magnetically ordered phase measured with the MERLIN chopper spectrometer. The inelastic spectra in the b^* direction recorded on MERLIN at T = 5 K with two incident energies of E_i = 25 meV and E_i = 10 meV are shown in Fig. 2 (a) and 2 (c) respectively. Given the low dimensional nature of the structure (further confirmed by the magnetic dynamics discussed in the supplementary information) we have integrated along the a^* and c^* directions. Figure 2 (a) displays a spin wave dispersion stemming from k=1, reaching a maximum top of the band at $\sim$ 12 meV. Higher resolution data taken with E_i = 10 meV displays an energy gap at the zone center of $\sim$ 2 meV, indicating an easy-axis anisotropy. Moreover, at k=1, the spin wave dispersion separates into two branches with a mode at 2 meV and a second one around 4 meV. The lower mode reaches a flat maximum at $\sim$ 3.5 meV while the higher mode disperses up to the 12 meV maximum observed on the E_i = 25 meV data. This separation is illustrated in the constant-Q cut k=1 displayed in Fig. 2 (e) (blue circles). In Fig. 2 (f), a constant-Q cut at k=1.5 shows the additional flat modes located near the magnetic zone boundary.

To understand the microscopic origin of these two modes and the dispersion, we have performed linear spin wave calculations based upon Heisenberg exchange and easy-axis anisotropy. As reported in the Cs counterpart [25], the nearest-neighbour interactions are dominated by super-exchange interactions, mediated by the F ions and are sensitive to distances and angles. Therefore, four different magnetic couplings are considered in this compound. The full spin Hamiltonian is written out in the supplementary information considering Fe-Fe nearest neighbour interactions mediated through Fe-F-Fe bonds. The four couplings constants considered are shown in Fig. 1 (a) and correspond to two intrachain couplings J_{ch1} and J_{ch2}, associated to Fe^{3+}-Fe^{3+} and Fe^{2+}-Fe^{2+} interactions, respectively, and two interchain couplings J_{int1} and J_{int2} associated to Fe^{3+}-Fe^{2+} interactions.

The calculations are illustrated in Figs. 2 (b) and 2 (d). Panel (b) illustrates a spin wave calculation where interchain interactions J_{int1},= J_{int2}=0 and panel (d) shows a calculation with both inter and intra chain interactions non zero. The band observed in the data for E_i = 25 meV (Fig. 2 (a)) corresponds to the dispersion along the Fe^{3+} b-axis chain as illustrated in panel (b) which was used to adjust the J_{ch2} intrachain coupling (indicated by the white arrows) and the easy-axis anisotropy associated with this site. The other terms of the spin Hamiltonian could be refined from the lower energy E_i=10 meV

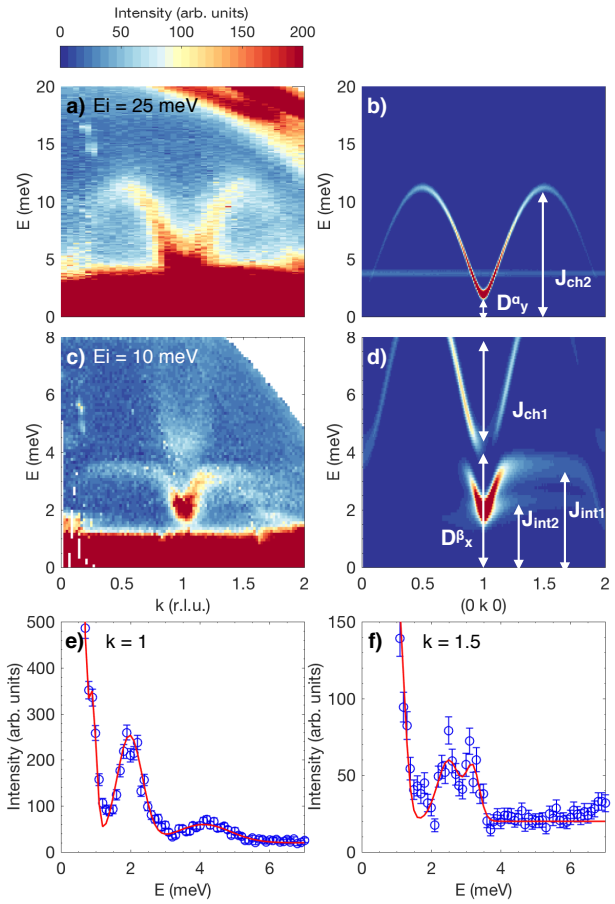

FIG. 2. (a), (c) Inelastic neutron scattering data of $RbFe_2F_6$ measured on MERLIN with incident energies of E_i = 25 meV and E_i = 10 meV at T = 5 K, along k. (b), (d) S(**Q**, ω) simulated with spinwave calculations along (0 k 0). The white arrows indicate the different fitted parameters. (e), (f) Constant-Q cuts along the k = 1 and k = 1.5 positions respectively. The red lines represent the fit of the energy position for the spinwave modes.

(Fig. 2 (c)) data. As displayed in Fig. 2 (d), the white arrows indicate how the energy position of the different modes allowed the refinement of the anisotropy term for Fe^{2+} and the three remaining exchange parameters. Notably, the anisotropy term affects the position of the higher mode and the slope of this branch is also affected by J_{ch1}. As for the flat modes near the zone boundary, their energy position is controlled by the interchain interactions J_{int1} and J_{int2}. Figures 2 (e) and (f) show a fit of the spin wave modes with chosen constant Q cuts at the zone center and near the zone boundary, respectively. The best solution found for the anisotropy terms is: D_y^{α} = 0.075 meV (for the Fe^{3}+ site) and D_x^{β} = 0.6 meV (for the Fe^{2+} site) in agreement with the difference in distortion between the $Fe^{3+}F_6$ and $Fe^{2+}F_6$ octahedra. The exchange couplings extracted from the fit are J_{ch1} = 1.40(5) meV (Fe^{2+} chain), J_{ch2} = 1.90(2) meV (Fe^{3+} chain), J_{int1} = 1.40(5) meV and J_{int2} = 0.75(10) meV.

The strongest coupling J_{ch2} is hence found along the Fe^{3+}-Fe^{3+} chain where the Fe-F-Fe angle is the closest to 180°. Describing the system as two interacting spin chains allows an understanding of the low-energy data: without the interchain interactions, the data in the k direction would only appear as a single mode stemming from $\vec{Q}$=(0 1 0) accounting for the dispersion of the Fe^{3+} chain (Fig. 2 (b)). Because of the interaction with the Fe^{2+} chain, the coupling between the two chains leads to the separation of the low-energy dispersion into two modes (Fig. 2 (d)), thus setting up two energy scales in the spin dynamics: one higher energy scale associated with the Fe^{3+} chain and a lower one tied to Fe^{2+} chain and the interchain interactions. As shown in the supplementary information, this lower energy mode is weakly dispersive for directions perpendicular to b. This is further confirmed by the temperature evolution of the spectra shown in Fig. 3. The interchain interaction was found to be of the order of 0.75 to 1.4 meV, which corresponds roughly to 8 to 15 K. Interestingly, near T_N at T = 15 K, the low energy data shows a collapse of the two modes, giving a single branch. Hence the interchain interactions are phased out by thermal fluctuations, and the only dominant energy scale remaining is the intrachain coupling between the Fe^{3+} ions. The inelastic signal also still shows a damped "dispersion" up to $2T_N\sim$ 30 K, indicating the persistence of short range spin correlations, a behavior characteristic of low dimensional systems [28, 29]. The persistence of short range correlations is consistent with the derived J_{ch2}=1.9 meV$\sim$ 22 K coupling between Fe^{3+} spins. The changes in the spin wave dispersion with temperature supports the energy scales derived from the low-temperature spin wave analysis. The temperature dependence also illustrates the underlying one dimensional nature of $RbFe^{2+}Fe^{3+}F_6$.

The noncollinear magnetic structure (illustrated in Fig. 1) brings the possibility for multi magnon states to be observable. In magnets with noncollinear spin structure, cubic anharmonic terms arise in the spin wave Hamiltonian due to the coupling of the transverse and the longitudinal fluctuations associated with deviations of the spin direction perpendicular and parallel to the ordered moment direction. These cubic terms have no analog in collinear magnets and describe the possibility of either an interaction between single and two magnons or the decay of single-magnons into pairs of other magnons [16, 31], giving rise to a continuum in the excitation spectrum. The continuum boundaries in energy and momentum are therefore determined by the q-dependence of the single-magnon dispersion affording such decay. We investigate the possibility of anharmonic or multiparticle excitations in $RbFe^{2+}Fe^{3+}F_6$ in Fig. 4 using spectroscopy data from MACS.

Fig. 4 (a) illustrates a contour map of the excitations

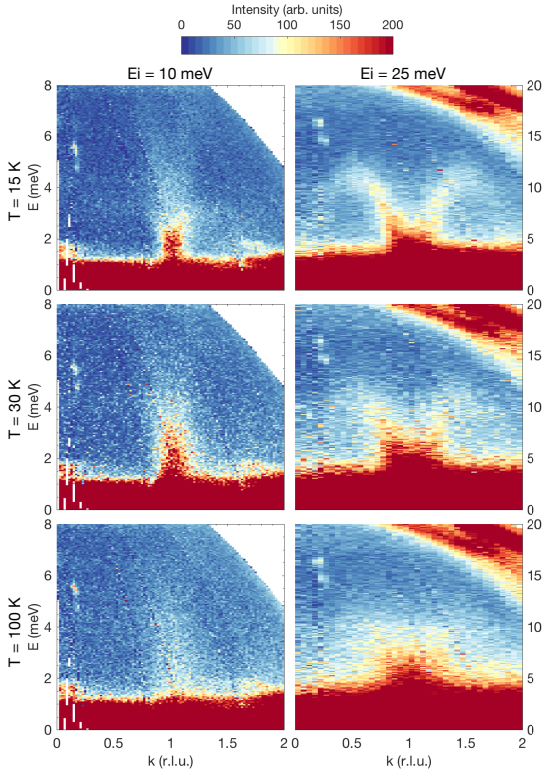

FIG. 3. Inelastic neutron scattering data of $RbFe_2F_6$ measured on MERLIN with incident energies of E_i = 10 meV (left) and E_i = 25 meV (right) along k at 15 K (top), 30 K (middle) and 100 K (bottom).

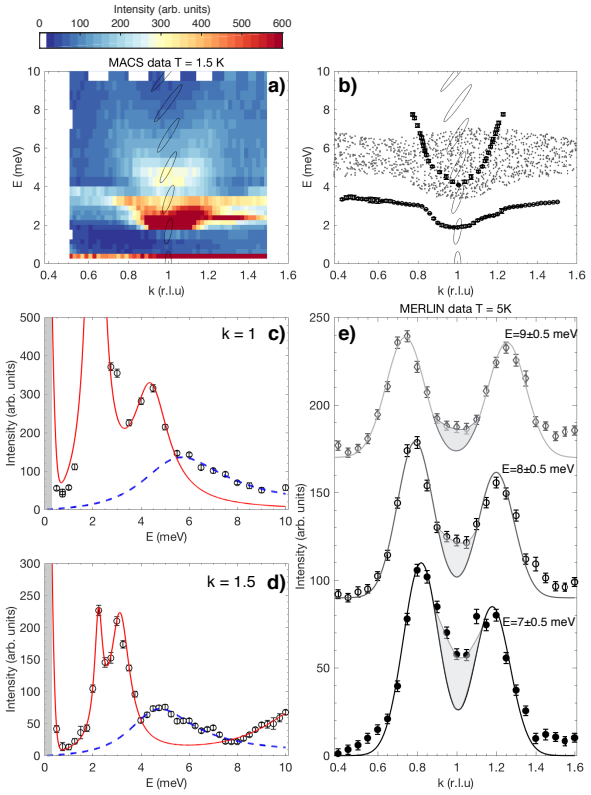

FIG. 4. (a) Inelastic neutron scattering data of $RbFe_2F_6$ measured on MACS with final energy of E_f = 3.7 meV along k at 1.5 K. The grey ellipses show the evolution of the resolution ellipsoid as a function of energy along the k = 1 cut, calculated with the RESLIB library [30]. (b) Two-magnon kinematic conditions calculated in the (E,Q) space (grey dots). The black circles are fits to the experimental data. ($c-d$) Constant k =1 and k = 1.5 cuts; the solid red line and blue dashed line show a fit to the data as described in the text. The grey area shows the energy resolution. (e) Constant E cuts recorded on MERLIN with E_i = 25 meV at 5 K.

measured on MACS with the peak of the dispersion illustrated by the solid points in Fig. 4 (b). The grey region in Fig. 4 (b) is the region where the Fe^{3+} spins are kinematically allowed to decay, conserving both momentum and energy, given the constraints of the low-energy branch. Fig. 4 ($c-d$) show constant -Q scans through the MACS data at the magnetic zone center (k=1) and the zone boundary (k=1.5). The sharp and intense single magnon excitations are seen at low energies but also an energy broadened component with comparable integrated spectral weight is observed up to high energies of $\sim$ 9 meV. This component is also extended in momentum as illustrated in panel (e) and is not associated with sharp single magnon excitations which are resolution limited in energy and momentum. The energy and momentum broadened cross section is not expected based on our single magnon analysis discussed above and the energy and momentum broadened nature indicates a shortened lifetime. The region in momentum and energy that this second component of scattering is observed does coincide with the expected energy and momentum region expected based on two magnons and the lower branch. Based on the broadened cross section and the comparison with calculations discussed above, we therefore conclude that this additional momentum and energy broadened component corresponds to the decay of Fe^{3+} excitations into multiparticle states.

This interpretation of a decay or leakage of Fe^{3+} excitations into a multiparticle continuum is also supported by magnetic diffraction data probing the magnetic structure. Given constraints of the total moment sum rule [33] of neutron scattering, the additional spectral weight appearing in the multiparticle continuum must draw from somewhere else in momentum and energy. As shown in classical, and collinear, Rb_2MnF_4[21] and quantum CFTD [20, 34], this spectral weight draws from the elastic channel in localized magnetic systems and this is consistent with the fact that neutron diffraction data reports a strongly reduced ordered moment for the Fe^{3+} site while not for the Fe^{2+}. As illustrated in Fig 4 (b) and given the kinematic conditions, the gap and energy range of the lower excitation mode provide favorable conditions to observe the decay of the higher energy Fe^{3+} excita-

tions.

Similar momentum and energy broadened continuum have been reported in quantum ($S = \frac{1}{2}$) [35, 36], itinerant magnets [37], and triangular systems [38, 39]. However, the observation of such a strong continuum and decay processes in a classical high spin magnet is unusual given predictions that such cross sections should scale as $\sim 1/S$ [17]. $RbFe^{2+}Fe^{3+}F_6$ is thus a unique case where charge ordering allows the coupling of non-collinear spins oriented 90° to each other and demonstrates that this multi magnon phenomenon is not constrained to purely quantum systems and extends to classical magnets. Such cross sections may be observable in other high spin magnets where similar "orthogonal" or noncollinear spin arrangements exist and may include the oxyselenides and oxysulfides [40–42]. The spin and charge degrees of freedom in $RbFe^{2+}Fe^{3+}F_6$ are well separated in terms of iron sites and also energy scales of branches. The multiparticle excitations may provide a means of coupling charge and spin degrees of freedom in $RbFe^{2+}Fe^{3+}F_6$ and similar coupling processes have been suggested in $BiFeO_3$ [43, 44] and low dimensional cuprates [45].

In summary, we report the magnetic fluctuations in charge ordered $RbFe^{2+}Fe^{3+}F_6$. The separation of different Fe^{2+} and Fe^{3+} chains results in an orthogonal spin arrangement on the two different magnetic sites and separate spin-wave branches. We observe multi magnon processes in this magnet and show that such processes can occur in classical magnets with a noncollinear spin arrangement.

We acknowledge funding from the EPSRC, STFC, and the Carnegie Trust for the Universities of Scotland. We are thankful to E. Cussen (Strathclyde) for fruitful discussion.

[1] F. C. Zhang and T. M. Rice, Phys. Rev. B **37**, 3759(R) (1988).
[2] P. W. Anderson, Science **235**, 1196 (1987).
[3] J. A. M. Paddison, M. Daum, Z. Dun, G. Ehlers, Y. Liu, M. B. Stone, H. Zhou, and M. Mourigal, Nat. Phys **13**, 117 (2017).
[4] T. H. Han, J. S. Helton, S. Y. Chu, D. G. Nocera, J. A. Rodriguez-Rivera, C. Broholm, and Y. S. Lee, Nature **492**, 406 (2012).
[5] M. A. de Vries, J. R. Stewart, P. P. Dean, J. O. Piatek, G. J. Nilsen, H. M. Ronnow, and A. Harrison, Phys. Rev. Lett. **103**, 237201 (2009).
[6] A. D. B. Woods and R. A. Cowley, Rep. Prog. Phys. **26**, 1135 (1973).
[7] A. J. Smith, R. A. Cowley, A. D. B. Woods, W. G. Stirling, and P. Martel, J. Phys. C: Solid State Phys. **10**, 543 (1977).
[8] B. Fak and J. Bossy, J. Low Temp. Phys. **10**, 543 (1977).
[9] S. E. Nagler, D. A. Tennant, R. A. Cowley, T. G. Perring, and S. K. Satija, Phys. Rev. B **44**, 12361 (1991).
[10] D. A. Tennant, T. G. Perring, R. A. Cowley, and S. E. Nagler, Phys. Rev. Lett. **70**, 4003 (1993).
[11] B. Lake, D. A. Tennant, C. D. Frost, and S. E. Nagler, Nat. Mater. **4**, 329 (2005).
[12] M. Enderle, B. Fak, H. J. Mikeska, R. K. Kremer, A. Prokofiev, and W. Assmus, Phys. Rev. Lett. **104**, 237207 (2010).
[13] F. Wilczek, Phys. Rev. Lett. **49**, 957 (1982).
[14] M. E. Zhitomirsky and A. L. Chernyshev, Rev. Mod. Phys. **85**, 219 (2013).
[15] A. Chernyshev and M. Zhitomirsky, Phys. Rev. Lett. **97**, 207202 (2006).
[16] A. Chernyshev and M. Zhitomirsky, Phys. Rev. B **79**, 174402 (2009).
[17] J. Igarashi, Phys. Rev. B **46**, 10763 (1992).
[18] J. Igarashi and T. Nagao, Phys. Rev. B **72**, 014403 (2005).
[19] I. Cabrera, J. D. Thompson, R. Coldea, D. Prabhakaran, R. I. Bewley, T. Guidi, J. A. Rodriguez-Rivera, and C. Stock, Phys. Rev. B **90**, 014418 (2014).
[20] N. Christensen, H. Rønnow, D. F. McMorrow, A. Harrison, T. Perring, M. Enderle, R. Coldea, L. Regnault, and G. Aeppli, PNAS **25** (2007).
[21] T. Huberman, R. Coldea, R. A. Cowley, D. A. Tennant, R. L. Leheny, R. J. Christianson, and C. Frost, Phys. Rev B **72** (2005).
[22] J. Oh, M. Le, J. Jeong, J.-H. Lee, H. Woo, W.-Y. Song, T. Perring, W. Buyers, S.-W. Cheong, and J.-G. Park, Phys. Rev. Lett. **111**, 257202 (2013).
[23] S. W. Kim, S.-H. Kim, P. S. Halasyamani, M. A. Green, K. P. Bhatti, C. Leighton, H. Das, and C. J. Fennie, Chem. Sci. **3**, 741 (2012).
[24] A. Abragam and B. Bleaney, Electron paramagnetic resonance of transition ions (OUP Oxford, 2012).
[25] M. V. Gorev, I. N. Flerov, A. Tressaud, E. V. Bodganov, A. V. Kartashev, O. A. Bayukov, E. V. Eremin, and A. S. Krylov, J. Solid State Chem. **237**, 330 (2016).
[26] M. S. Molokeev, E. Bogdanov, S. Misyul, A. Tressaud, and I. Flerov, J. Solid State Chem. **200** (2013).
[27] S. Petit, Collection SFN **12**, 105 (2011).
[28] T. Huberman, D. A. Tennant, R. A. Cowley, R. Coldea, and C. D. Frost, J. Stat. Mech. Theor. Exp. **5**, 1742 (2008).
[29] F. Demmel and T. Chatterji, Phys. Rev. B **76** (2007).
[30] A. Zheludev, ResLib 3.4, Oak Ridge National Laboratory, Oak Ridge, TN (2007).
[31] M. Mourigal, W. Fuhrman, A. Chernyshev, and M. Zhitomirsky, Phys. Rev. B **88**, 094407 (2013).
[32] L. P. Pitaevskii, JETP **36**, 830 (1959).
[33] P. C. Hohenberg and W. F. Brinkman, Phys. Rev. B **10**, 128 (1974).
[34] B. Dalla Piazza, M. Mourigal, N. B. Christensen, N. G.J., P. Tregenne-Piggott, T. G. Perring, M. Enderle, D. F. McMorrow, D. A. Ivanov, and H. M. Ronnow, Nature Physics (2014).
[35] M. B. Stone, I. A. Zaliznyak, T. Hong, C. L. Broholm, and D. H. Reich, Nature **440**, 187 (2006).
[36] T. Masuda, Z. Zheludev, H. Manaka, L. P. Regnault, J. H. Chung, and Y. Qiu, Phys. Rev. Lett. **96**, 047210 (2006).
[37] C. Stock, J. A. Rodriguez-Rivera, K. Schmalzl, E. E. Rodriguez, A. Stunault, and C. Petrovic, Phys. Rev. Lett. **114**, 247005 (2015).
[38] R. Coldea, D. A. Tennant, and Z. Tylczynski, Phys. Rev.

B **68**, 134424 (2003).
[39] D. Dalidovich, R. Sknpenek, A. J. Berlinsky, J. Zhang, and C. Kallin, Phys. Rev. B **73**, 184403 (2006).
[40] L. L. Zhao, S. Wu, J. K. Wang, J. P. Hodges, C. Broholm, and E. Morosan, Phys. Rev. B **87**, 020406 (2013).
[41] E. E. McCabe, C. Stock, E. E. Rodriguez, A. S. Wills, J. W. Taylor, and J. S. O. Evans, Phys. Rev. B **89**, 100402(R) (2014).
[42] C. Stock and E. E. McCabe, J. Phys.: Condens. Matter **28**, 453001 (2013).
[43] M. O. Ramirez, M. Krishnamurthi, S. Denev, A. Kumar, S. Y. Yang, Y.-H. Chy, E. Saiz, J. Seidel, A. P. Pyatakov, A. Bush, D. V. J. Orenstein, R. Ramesh, and V. Gopalan, Appl. Phys. Lett. **92**, 022511 (2008).
[44] M. O. Ramirez, A. Kumar, S. A. Denev, Y. H. Chu, J. Seidel, L. W. Martin, S. Y. Yang, R. C. Rai, X. S. Xue, J. F. Ihlefeld, N. J. Podraza, E. Saiz, S. Lee, J. Klug, S. W. Cheogn, M. J. Bedzk, O. Auciello, D. G. Schlom, J. Orenstein, R. Ramesh, J. L. Musfeldt, A. P. Litvinchuk, and V. Gopalan, Appl. Phys. Lett. **94**, 161905 (2009).
[45] C. Hess, H. ElHaes, B. B. U. Ammerahl, M. Hucker, and A. Revcolevschi, Phys. Rev. Lett. **93**, 027005 (2004).